Journal of Solar Energy Research (JSER)

Journal homepage: www.jser.ut.ac.ir

Peak Flux Density Comparison on the Receiver Image between Conventional and Rotating Heliostats

Messaoud Bouamra[a,*], Ahmed Dahia[b]

[a] *Department of Mechanical Engineering, Faculty of Sciences and Technology, Ahmed Zabana University of Relizane, Algeria.*
[b] *Nuclear Research Center of Birine, B.P. 180, AIN OUSSERA 17200, Djelfa, Algeria.*

ARTICLE INFO

Article Type:

Research Article

Received: 2025.07.05
Accepted in revised form: 2025.09.10

Keywords:
Cavity receiver;
Power tower;
Simulation;
Solar;
Rotating heliostat field

A B S T R A C T

The current study uses the HFCAL approach to construct a computing algorithm that provides the flux density distributed on the receiver image of a northern hemisphere heliostat. As part of the flux computation process, optical performance was improved by replacing the conventional heliostat with a rotating model that optimizes the cosine effect. The results obtained were validated against experimental data from the solar platform plant in Almeria, Spain. The concentrated solar flux incident on the receiver surface from the two technologies, conventional and rotating heliostats, is compared at five specific times on the spring equinox day. The comparison is carried out for both a single heliostat and a group of heliostats similar to those in the PS10 tower field. The results show that rotating heliostats significantly outperform conventional systems, particularly during the morning and afternoon when the sun is at lower altitudes and precise tracking is critical. At 08:00, the peak flux density increases by 36.25% compared to a conventional heliostat row, while at 10:00 and 14:00 the improvement is 12.38% for both times. At solar noon, both systems achieve similar peak flux values. This demonstrates higher peak flux and more uniform illumination in a simplified solar field.

1. Introduction

The economic prosperity of nations worldwide is adversely affected by the environmental impact of fossil fuel energy systems. One highly effective strategy to reduce excessive dependence on fossil fuels while addressing the growing energy demand is the adoption of renewable energy sources, particularly solar energy [1-3].

*Corresponding Author Email:bouamram@gmail.com

Cite this article: Bouamra, M. and Dahia, A. (2025). Peak Flux Density Comparison on the Receiver Image between Conventional and Rotating Heliostats. Journal of Solar Energy Research, 10(2), 2335-2348. doi: 10.22059/jser.2025.398075.1592

DOI: 10.22059/jser.2025.398075.1592

Interest in solar tower power station technology, as one of many renewable technologies that have great potential to substitute the increasing demand for conventional energy[4, 5], began to grow significantly in the early 2000s with the design of the PS10 (Solar One) plant in Spain that started operation in 2007. Since then, tower technology has continued to undergo remarkable evolution with their new projects[6].The American Ivanpah Solar Tower Power Plant, located in California's Mojave Desert, which has a generating capacity of 392 megawatts of electricity, has even become the world's largest operational concentrating solar thermal plant since it was commissioned in December 2013 [7].In recent years, other developing countries such as Morocco, Chile, China, and South Africa have attracted significant investments, largely supported by international organizations [8, 9].

Common solar tower power stations are delicate assemblies that frequently have three subsystems: a heliostat field, a tower with a receiver, and a power converter system[10, 11]. The heliostat field, which is a large number-tracking reflector, reflects and focuses direct solar radiation onto a receiver at the top of the tower. In the receiver, a generated thermal heat is delivered by a heat transfer fluid to the power conversion system to produce electricity or any other types of heat applications [12-14].

Of these three subsystems, the heliostat field is responsible for around half of the investment cost of the power plant [7, 14]. However, to reduce the high prices of heliostats, it is essential to optimize the field layout, which means improving the power output by using a small number of heliostats over a small field area as possible. Several design elements can be optimized to prevent the system cost from increasing with each new heliostat in the field [13, 15]. Power tower plants can use three of the most popular heliostat technologies: pillar heliostats, tissue heliostats, and rotating heliostat fields [7].

Presently, the solar power tower plant operates with a stationary receiver at the top of the tower and a field of heliostats anchored to the ground referred to as conventional heliostats .Each heliostat is generally defined as a device containing several reflecting mirrors, mounted on a movable support, which must follow the sun on its path during the day and reflect the sunlight in a fixed direction toward the receiver.While rotating heliostats, also called helio-mobiles[11], are one of the earliest designs that are arranged into concentric rails, where they move around the tower in an automated way to follow the apparent movement of the sun throughout the day, as illustrated in Figure 1. In contrast to the conventional heliostat, which rests on a concrete base that limits its tracking ability, these helio-mobiles are built over a mobile platform that offers more dynamic and continuous tracking. Thus, the heliostats are located east of the tower at sunset, north at solar noon and west at sunrise, in a receiver that faces north. In this context, Ruiz et al. (2014) [16] described this new concept of a rotating heliostat field that has been developed and built by the Spanish research center Advanced Technology Center for Renewable Energy (CATER) in Tabernas. Cadiz et al. [17] presented one of the first studies on the rotating heliostat concept, developing a code to optimize azimuthal distances and reduce shadowing and blocking losses. Their work, and a few related studies, mainly focused on optical efficiency and field layout. However, the flux density distribution on the receiver under rotating heliostat configurations is not explored. A recent study by the present author demonstrated significant improvements in the optical efficiency of solar fields using the rotating heliostat concept. Building upon these efforts [10, 18] , the current paper advances the research by analyzing flux density distribution and developing a rapid preliminary method for simulating the solar flux incident on the receiver surface.

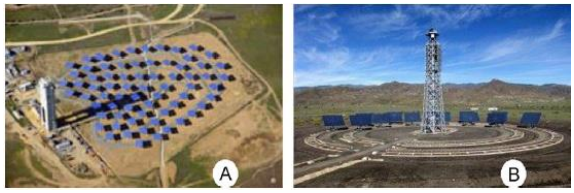

Figure 1. (A) Conventional heliostat field at the Solucar Platform(B) Rotating heliostat field at CTAER [11]

The receiver at the top of the tower is the optical structure interface between the heliostat field and a power conversion system [19]. System design parameters for solar power towers also include the computed maximum flux produced by the collector field on the receiver surface. It is typically set to a maximum value to avoid thermal stresses and physical damage to the receiver pipes [20].The distribution of solar flux in the receiver has been exposed through a number of simulated and experimental investigations [21]. They can be basically classified into two distinct groups: ray tracing and convolution methods. The first one is a statistical approach that draws a random beam of the sun's rays to provide an accurate map of the flux distribution, and it requires higher computational

cost [22]. The second method depends on the mathematical superposition of several errors, including the error in the shape of the sun, the inconsistency and the reflecting surface's quality and the accuracy of the sun monitoring system [23, 24]. Many techniques have been proposed to resolve the integral of convolution, some of which are HFLCAL, UNIZAR and iHFLCAL as described in [24]. Lipps and Walze [25] developed an analytical expression on non-focusing heliostats. Collado et al. [26] introduced an error function that leads to a simple analytical expression governing focusing heliostats, which has recently become known as UNIZAR [20]. Another approximate solution that is simpler and more accurate than the previous one[22] assumes Gaussian behavior for all error cones; this is the model HFLCAL [20] of the Aerospace Center of Germany. The accuracy of analytical approaches is generally lower than that of ray tracing, but good enough for most applications requiring fast optimization[20, 25].

In this study, the peak flux density distribution produced by two different technologies, namely conventional and rotating heliostats, is compared using a limited number of these devices to quickly optimize the solar flux distribution on the receiver's image plane. The heliostats under investigation are well suited for the HFLCAL technical method, which computes the distribution of the flux density on the receiver. An algorithm in the MATLAB environment has been developed and validated with the experimental data available from the Solar Platform plant in Almeria in Spain [20]. For this, the first row of 9 heliostats of the PS10 [10] was considered. At specific times in spring equinox, the flux maps are finally generated on the receiver and some conclusions are drawn.

2. Model description

2.1. Coordinate system

As illustrated in Figure 2, the first global coordinate system (O, X, Y, Z) has its origin O in the tower base at ground level [27].The second coordinate system (H, U, V, W) [23] is linked to the heliostat frame, where the center of the reflective surface H is the origin, and W is normal for both axes U and V belonging to the heliostat surface. The third coordinate system (I, x_r, y_r, z_r)is related to the receiver image plane, where I is the center of the receiver and z_r is normal to the plane formed by x_r and y_r axes [21].The radiation distribution on the surface of the receiver is simulated with HFLCAL as indicated below.

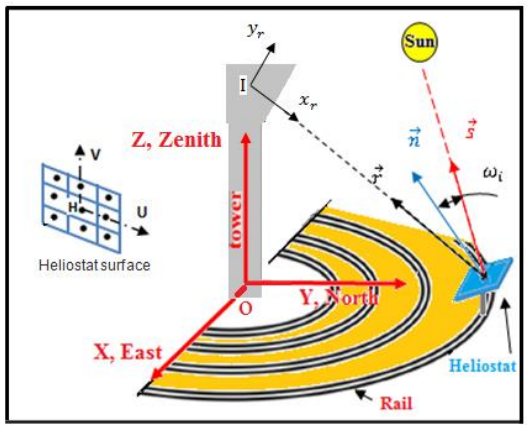

Figure 2. Heliostat location

2.2. HFLCAL model

The resolution of the algebraic expression of the HFLCAL method, which forms the basis of our model, takes into account all causes of image deformation, including the shape of the sun, the quality of the mirrors of the heliostats, as well as the tracking errors of the image. This method's accuracy has made possible to obtain the distribution of the solar energy flux reflected by the heliostat to the receiver. This model is based on the theoretical principle that the spot of the sun on the surface of the receiver follows a Gaussian normal distribution law[28] , that is to say [22]:

$$F(x_r, y_r) = \frac{P_t}{2\pi\sigma_{HF}^2} . \exp\left(-\frac{(x_r - x_v)^2 + (y_r - y_v)^2}{2.\sigma_{HF}^2}\right) \quad (1)$$

With F, the shape of the sun image on the receiver; x_r , $y_r$the coordinates of the points of the receiver plane in the coordinate system linked to the receiver;x_v , y_v the coordinates of the aiming point of the center of the heliostat on the receiver and $P_t$the solar power reflected by the heliostat , given as [29]:

$$P_t = I_D . \rho . \cos\omega_i . A_m . f_a \quad (2)$$

Where I_D is the direct solar irradiation (KW/m^2); A_m is the total mirror area of heliostat; $\cos\omega_i$ is the cosine effect; f_a is the atmospheric attenuation factor and ρ is the effective reflectivity of the mirror.

The effective deviation σ_{HF}, is the convolution of the four Gaussian error functions, namely, the sun

shape error (σ_{sun}), the beam quality error (σ_{bq}), the astigmatic error (σ_{ast}), and the tracking error (σ_t) [29]. σ_{HF} is given as[2] :

$$\sigma_{HF} = \frac{\sqrt{D^2\left(\sigma_{sun}^2 + \sigma_{bq}^2 + \sigma_{ast}^2 + \sigma_t^2\right)}}{\sqrt{cosrec}} \quad (3)$$

Where D is the distance between the center of the reflective surface and the target point[2], and cosrec represents the cosine of the angle between the reflected ray and the normal to the receiver surface. The beam quality error is due to defects of the reflective surface and is linked to the slope error by [29]:

$$\sigma_{bq} = (2\sigma_s)^2 \quad (4)$$

The standard deviation of the astigmatic error is given as [20]:

$$\sigma_{ast} = \frac{\sqrt{0.5(H_t^2 + H_s^2)}}{4D} \quad (5)$$

Where H_t and W_s are the image dimensions in the tangential and sagittal plane and are given as [20]:

$$H_t = d\left|\frac{D}{f} - \cos\omega_i\right| \quad (6)$$

$$W_s = d\left|\frac{D}{f}\cos\omega_i - 1\right| \quad (7)$$

Where, f is the focal distance, and d is a general dimension of the heliostat. This work has assumed that d is equal to the square root of the whole heliostat area [30, 31], which is defined as:

$$d = \sqrt{H_w \times H_h} \quad (8)$$

Where H_w and H_h are the width and the height of the heliostat, respectively.

2.3 Optimization of the cosine effect

The cosine factor is one of the most important parameters for increasing the solar field's optical efficiency. Although multiple factors influence the overall efficiency, the cosine effect has a particularly significant impact on the final result [15]. Optimizing this factor directly improves the instantaneous optical efficiency (η) of the heliostat field, which is determined by the product of several efficiency components, as expressed by [13]:

$$\eta = \eta_{cos} \cdot \eta_{sb} \cdot \eta_{itc} \cdot \eta_{att} \cdot \eta_{ref} \quad (9)$$

Where: η_{cos} represents cosine efficiency, η_{sb} accounts for shading and blocking, η_{itc} is the interception of sun rays at the aperture, η_{att} is atmospheric attenuation, and η_{ref} is heliostat reflectivity.

The cosine efficiency depends on the incidence angle,ω_i, which is the angle formed between the direction of incoming solar radiation and the perpendicular (normal) to the heliostat surface[10]. This phenomenon is depicted in Figure 3 by showing conventional heliostats located at two different points within the solar field. Heliostat A, located on the right side of the field, has a lower cosine loss than Heliostat B on the left. This is due to its smaller incidence angle,ω_i, resulting from a more favorable orientation for reflecting sunlight toward the receiver. As a result, heliostat A achieves higher optical efficiency in the morning, while heliostat B has greater losses at that time but lower losses in the afternoon as the sun's position changes. In comparison, the current optimization shown in Figure 4 represents a rotating heliostat, which overcomes the limitations of conventional heliostats by continuously adjusting its orientation to remain optimally aligned with the sun's azimuth. This tracking feature helps maintain a low incidence angle throughout the day, thereby ensuring more stable and efficient cosine performance, increased solar energy capture, and improved optical performance.

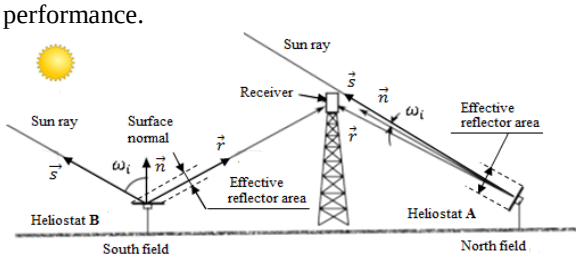

Figure 3.Cosine losses for a conventional heliostat in the field [32]

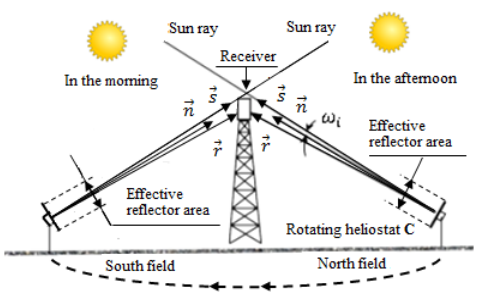

Figure 4.Cosine losses for rotating heliostat in the field (Our optimization).

The cosine efficiency can be simply calculated by the following relation [10]:

$$\eta_{cos} = \vec{n}.\vec{s} \quad (10)$$

Where $\vec{s}$ is the solar vector and $\vec{n}$ the surface normal vector. In a conventional heliostat field, the distribution of heliostats is determined by the fixed coordinates of their centers, which are defined by their radial distance and angular position relative to the tower and remain constant. For rotating field, the heliostats move along circular rails around the tower, dynamically updating their coordinates. The algorithm created for the specified task was described using the flowchart of Figure 5.

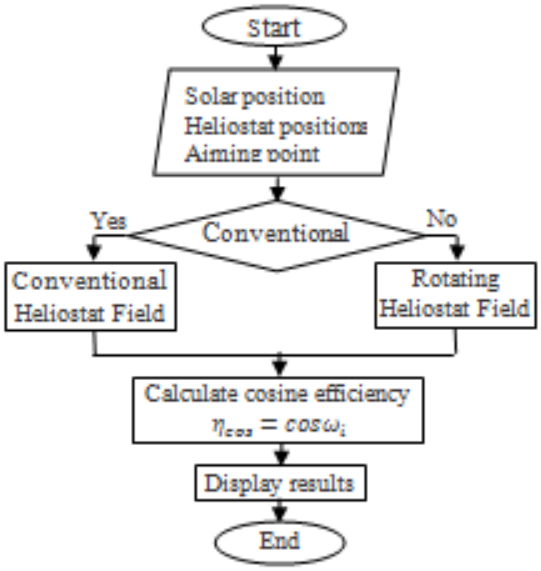

Figure 5. Flowchart of solving cosine efficiency

2.4 Comparison of Solar Flux at the Receiver

The HFCAL method compares the incident solar flux from the two types of heliostats reaching the receiver surface. One heliostat and a group of heliostats are compared using the two different forms of technology. The plant model used is based on the PS10 tower field. The aim point is the center of the image plane of the receiver. A parabolic reflecting surface shape of rectangular section and ideal focal length models each heliostat. It is assumed that the slope error σ_s is 1 mrad [29] and both tracking and atmospheric attenuation errors are neglected. Therefore, no attention is dedicated to the geometrical characteristics of the receiver, which is considered as the image plane whose normal matched the reflective ray vector.

3. Results and discussion

3.1 Validations

Firstly, the redesign of the conventional heliostat field is based on the geometric center coordinates of the heliostats in the PS10 commercial field, as described in Ref. [33].The slope of the land of the heliostats field is defined as zero and each heliostat is at the same altitude. The design point was the spring equinox noontime and the parameters used on the model are depicted in Table1.

Table 1.Parameters of PS10 heliostat field [10, 33]

Parameters	Value
latitude	37.4°N
longitude	-6.25°
Field shape	Rotating field
Layout way	Radial staggered
Heliostat width H_w	12.84 m
Heliostat height H_h	9.45 m
Heliostat center height, h	5.17 m
Heliostat number, n_h	624
Target center X_r, Y_r and Z_r coordinates (m)	(0, 0, 100.5)
Tower length	18 m
Tower width	8 m
Sun shape error σ_{sun}	2.51(mrad)
Mirror slope error in HFCAL model σ_{s-HF}	1 (mrad)

In order to verify the correctness of our model, our program computes the cosine efficiency of the conventional field and compares the findings with a previous works in reference [34], as indicated in Table 2.

Table 2. Average cosine efficiency of PS10 conventional and rotating heliostat fields

	Original PS10 field [34]	Conventional PS10 field	Rotating PS10 filed
Average cosine efficiency (%)	82.83	88.06	94.57

The differences between the results are mainly explained as follows: Firstly, the average cosine efficiency is 5.23%, as it was calculated for the entire field only on the spring equinox, with an

assumed operating time from 08:00 to 16:00, instead of using a yearly average. This choice was made to reduce the time required for preliminary optimization. Regarding the assumptions taken in this work, our results agree strongly with those published by Saghafifar et al. [34]. Secondly, the PS10 rotating field performs better than the original PS10 configuration in terms of average cosine efficiency, as its heliostats continuously adjust to the sun's position, maintaining optimal reflection angles throughout the day. However, this improved tracking efficiency comes at the cost of increased land use, since the rotating field requires heliostats to move along circular paths around the tower, resulting in a larger occupied area compared to the conventional field. Figures 6, 7 and 8 provide a more detailed explanation of the relationship between cosine efficiency and the land area occupied by the rotating heliostat field at 8h, 10h and 12 h solar time , respectively, over a whole spring equinox day . The heliostats were colored on their efficiency levels. The green color indicates the range less than 0.90 and the red one is the maximum value of efficiency greater than 0.98. Symmetry is observed in the variation of heliostat position and cosine efficiency relative to solar noon throughout the day.

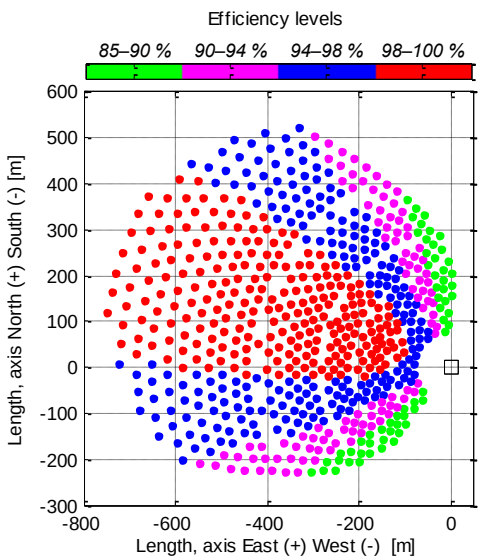

Figure 6. Cosine efficiency distribution of 624 heliostats at 8:00 h in the simulated PS10 rotating field around the tower located at point (0, 0).

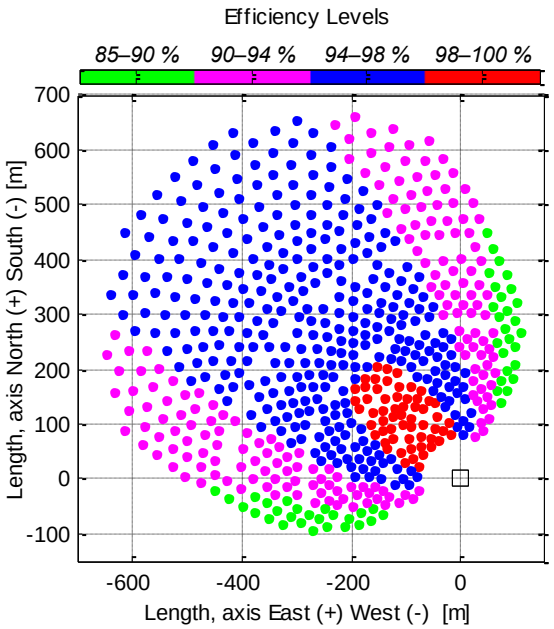

Figure 7. Cosine efficiency distribution of 624 heliostats at 10:00 h in the simulated PS10 rotating field around the tower located at point (0, 0).

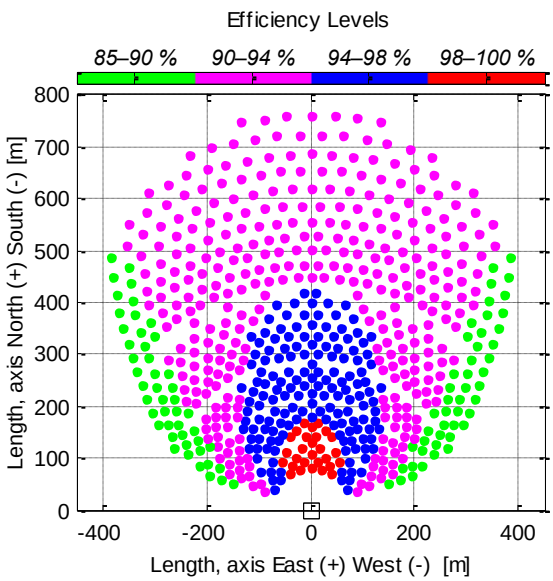

Figure 8. Cosine efficiency distribution of 624 heliostats at 8:00 h in the simulated PS10 rotating field around the tower located at point (0, 0).

The flux density model's accuracy was confirmed by experimental measurements taken from the Solar Platform plant in Almeria, Spain [20]. Every heliostat contains 12 spherical faces (1.105 × 3.010 m) [29] ,and the heliostat's overall mirror area is 39.9126m^2 [35]. The vertical flat plate, which is considered as the receiver, is 35.16 meters high. The selected heliostat parameters and the tower system are reported in Table3.

Table 3.Parameters of the selected PSA heliostat and tower system [20, 29]

Parameters	Value
Day of test	9 of July 2004
Time(UT)	11 :43 :21
DNI(KW/m^2)	1
Heliostat name	C1
Heliostat X, Y and Z coordinates (m)	(-64.02, 150.26, 6.06)
Whole area of the heliostat A_h (m^2)	45.536
Heliostat width H_w (m)	6.6778
Heliostat height H_h (m)	6.819
Receiver width R_w (m)	8.0
Receiver height R_w (m)	7.2
Target center coordinates (m)	X_r, Y_r and Z_r (0, 0.74, 35.16)
Attenuation factor f_{att}	1
Mirror reflectivity factor ρ	1
Sun shape error σ_{sun} (mrad)	2.51
Mirror slope error in HFCAL model σ_{s-HF} (mrad)	1.19
Tracking error σ_t (mrad)	0
Incidence cosine $cos\omega_i$	0.8477
Distance between the heliostat surface center and the aim point D(m)	165.23
Focal length f(m)	166.6

Eq. (1) and the HFLCAL approach are used to create the model in the MATLAB environment that provides the flux density of the heliostat. Figure 9 depicts the distributions of the measured flux densities on the target surface (PSA), and the results obtained through numerical simulation using the proposed C1 heliostat model [20]. As can be seen, the analytical method cannot precisely predict the actual form of the flux density based on the symmetry assumption of the curve's shape, which follows the law of a circular Gaussian distribution, but it is able to provide an accurate value of the maximum flux. A systematic comparison of the flux peaks is presented in Table 4.

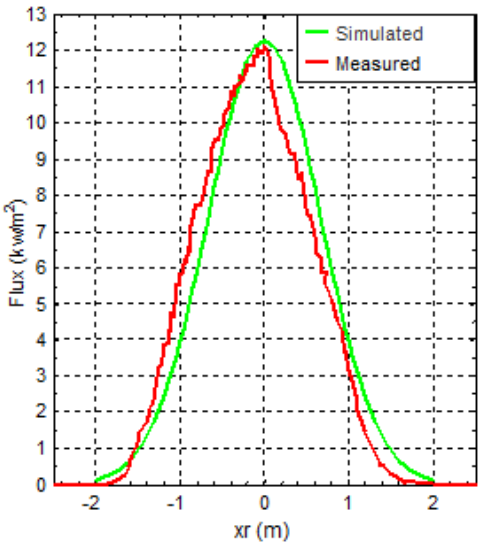

Figure 9. Measured [20] and simulated Central profiles ($y_r = 0$) of flux density for heliostat C1 aim at the center of the receiver in PSA power plant.

Table 4.Measured [20] and simulated flux peaks (kW/m^2)

Models	Measured [20]	Simulated
Peaks of flux (kW/m^2)	12.11	12.25

The differences in the flux peaks between the simulated and the measured [20] models are 0.14 (kW/m^2), which means that the results are in good agreement with those published by Collado [20]. It is also noted that the suggested model is highly effective and safe to use with confidence for the conventional and rotating heliostats. In this validation case, the assumption of zero tracking error is justified by the short slant range (≈165 m) and the relatively large receiver dimensions (7.2 m × 8 m), which minimize the effect of misalignments. According to literature[36], modern heliostat systems can achieve tracking accuracies better than 1 mrad, corresponding to about 2 m displacement of the focal point at a slant range of 1 km . At our shorter distance, the effect is negligible. This assumption is also consistent with simplified flux models such as HFCAL, where peak-flux fitting is sufficient for accurate validation.

3.2 Solar Flux from Rotating and Conventional Heliostats

In this section, two cases are studied with the same basic configuration. Case A, is a small tower solar power plant, but under the theoretical approach described above, it is assumed that only a single

heliostat rotates following the path of the sun. The heliostat moves from the first position to the fifth on a circular path with the tower at the center as shown in Figure 10, and does so at the same speed as the variation of the solar azimuth. Case B is the same installation with a field of conventional heliostats. Five conventional heliostats are selected from the first line of the PS10 tower field for the evaluation. They have been organized so that the rotating heliostat of case 1 occupies the same position with each of them, moving from the first position at 8:00 to the fifth position at 16:00 (solar time) at two-hour intervals, as shown in Figure 11. A set of sun positions, the corresponding angles of azimuth and elevation, and the position of a rotating heliostat are presented in Table 5.

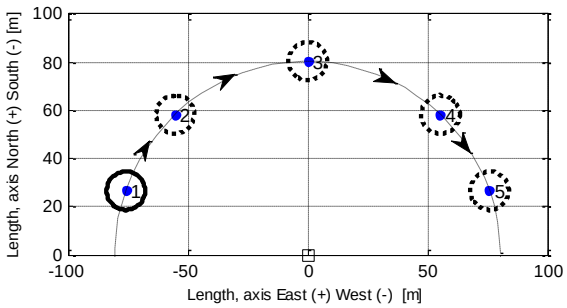

Figure 10. Rotating heliostat around the tower at (0,0), positions 1–5. Solid circle: current position; dotted circles: future positions; movement follows solar azimuth.

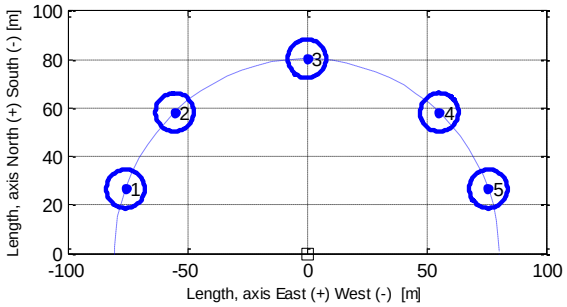

Figure 11. Five conventional heliostats around the tower at (0,0) selected from the first row of the PS10 field.

Table 5. Elevation, azimuth angles, and positions of a rotating heliostat at five solar times on the spring equinox day

Solar time	8h	10h	12h	14h	16h
Elevation angle [°]	23.39	43.44	52.56	43.44	23.39
Azimuth angle [°]	- 70.66	- 43.52	0.00	43.52	70.66
Position	1	2	3	4	5

Figure 12 shows the variation of peak flux values produced by the rotating heliostat and the set of five conventional heliostats on the receiver image plane located at coordinates (0, 0, 100.5). The results are presented for five solar times [h] of the spring equinox day: 8:00, 10:00, 12:00, 14:00, and 16:00.

From these data, symmetry is observed in the evolution of the value of the peak flux relative to noon along the day. The rotating heliostats have improved focusing capabilities with higher and sharper peak flux compared to standard designs, likely due to better tracking or optical alignment. The highest and lowest values are 113.18 (kW/m²) and 105.73 (kW/m²), respectively. The range of 7.45 from the lowest to the highest values, a small fluctuation, could indicate that the system offers more dynamic and continuous tracking as the solar mirrors reflect it to be more precisely aligned with the sun's rays.

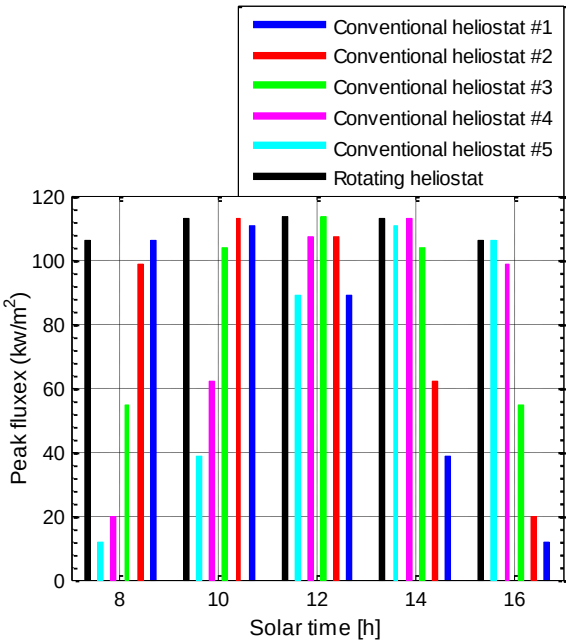

Figure 12. Variation of peak flux values on the receiver image plane located at point (0, 0, 100.5) for different solar times [h] (8, 10, 12, 14, 16) during

the spring equinox day, comparing one rotating heliostat to five conventional heliostats.

3.3 Superimposed flux from rotating and conventional heliostats

For this comparison, the basic configuration selected for the group of heliostats is a small field of 9 heliostats, which is similar to the first row from the tower of the PS10 solar power plant. Like the previous subsection, two cases are studied, both with the same basic configuration. Case C is a small tower solar power plant with a row of 9 conventional heliostats that are similar to those existing in the PS 10 tower field, as seen in Figure 13.Case D is the same installation as the previous one, but under the technology to rotate the entire field of nine heliostats following the sun's path. Thus, in the northern hemisphere, as illustrated in Figures 14(a-e), these heliostats are situated east of the tower at sunset, north at noon and west at sunrise. The design point was the spring equinox with five solar time points: 8 h, 10 h, 12 h, 14 h and 16h, respectively. A set of sun positions is illustrated in Figure 15.

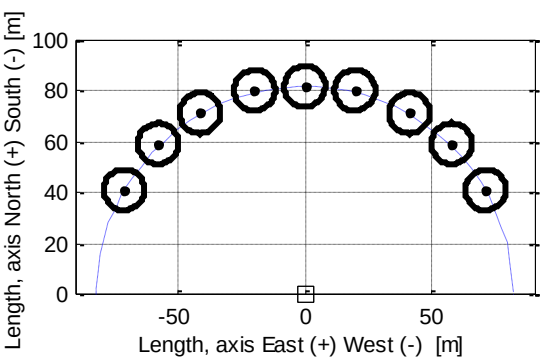

Figure 13. Arrangement of nine conventional heliostats around the tower located at point (0,0), as in the first row of the existing PS10 solar power plant, all aimed at the receiver's midpoint

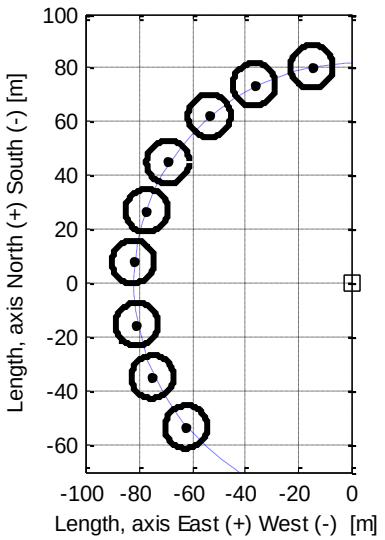

Figure 14(a). Position of nine rotating heliostats around the tower at 08:00, representing an equivalent rotating field of the first row of the PS10 solar field.

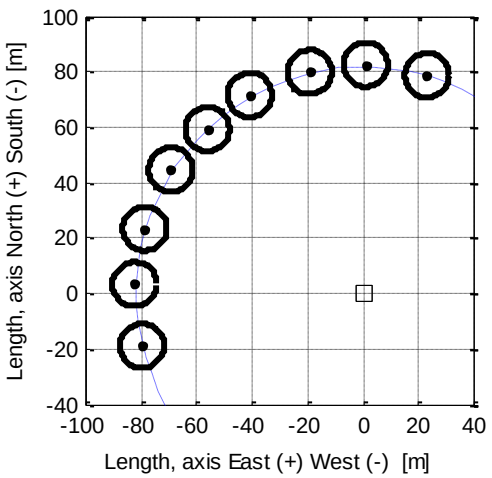

Figure 14(b). Position of nine rotating heliostats around the tower at 10:00, representing an equivalent rotating field of the first row of the PS10 solar field

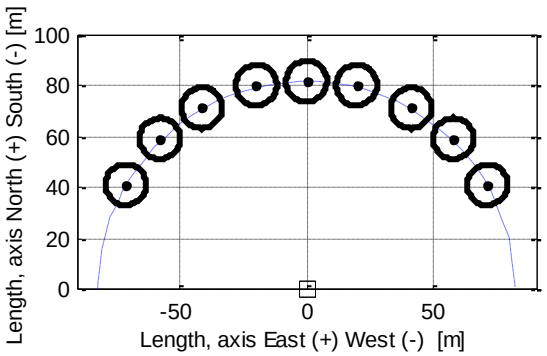

Figure 14(c). Position of nine rotating heliostats around the tower at 12:00, representing an equivalent rotating field of the first row of the PS10 solar field.

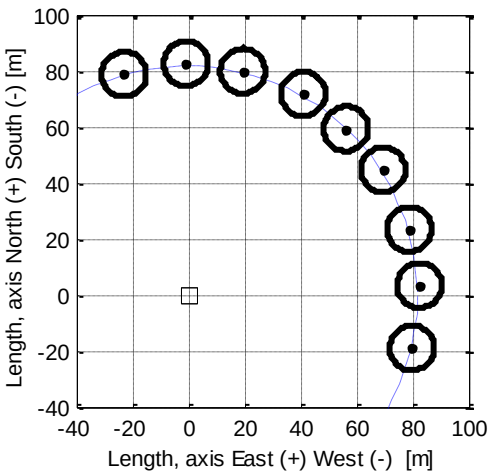

Figure 14(d). Position of nine rotating heliostats around the tower at 14:00, representing an equivalent rotating field of the first row of the PS10 solar field

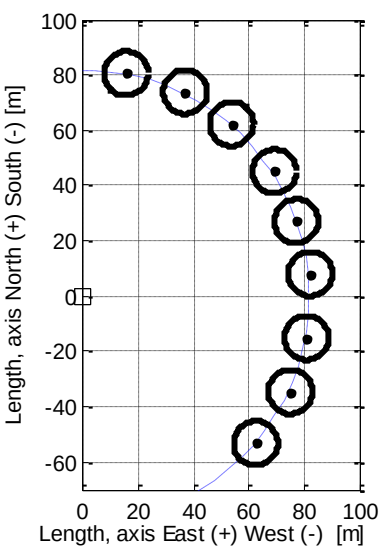

Figure 14(e). Position of nine rotating heliostats around the tower at 16:00, representing an equivalent rotating field of the first row of the PS10 solar field.

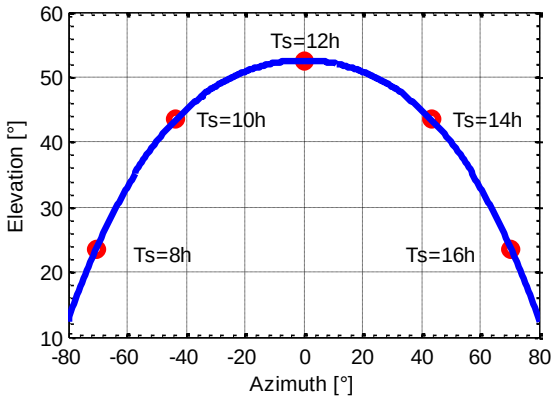

Figure 15. Sun trajectory and positions during the spring equinox day at the PS10 solar field location in Spain.

Figure 16 show the superposition of the peak flux density distribution on the receiver's image plane sent by two groups of conventional and rotating heliostats from 8 a.m. to 4 p.m. on the spring equinox day, where all the heliostats are aimed at the receiver's midpoint. The first group is just the first row of the existing PS10 solar power plant in Spain, "Case C," and the second is an equivalent rotating solar field concept, "Case D". The comparison shows that both systems have a similar ability to direct solar energy onto the receiver surface, especially around midday, when the sun is at its highest position. At noon (12.00), both systems provide the same peak flux around 950.81 kW/m² and show equal interception efficiency. However, during the morning and afternoon hours, the rotating heliostat row provides a higher peak flux. At 8 a.m. and 4 p.m., the rotating heliostat row reaches 804.35 kW/m², while the conventional one reaches only 512.74 kW/m², a difference of about 36.25 %. At 10 a.m. and 2 p.m., the values are 930.45 kW/m² for the rotating row and 815.24 for the conventional row, with a 12.38 % advantage for the rotating system. These differences show that the rotating heliostat is more effective at concentrating sunlight when the sun is at a low angle. A closer look at the width of the flux distribution shows a slight difference in the interception efficiency. At 8 a.m. and 2 p.m., the rotating row shows intercepted solar rays over a range of 5.0 m, while the conventional row covers 4.6 m, a difference of about 8 %. By 10 a.m. and 2

p.m., both curves extend over almost the same surface area of the receiver, showing interception widths of about 5.0 m for both systems meaning the interception efficiency becomes nearly identical at that time. These results mean that the rotating heliostat sends more concentrated energy to the receiver, when the sun is at a low angle. This improvement arises from better optical alignment, which reduces cosine losses and maintains sharper focusing conditions outside solar noon. Nevertheless, these optical advantages involve practical trade-offs: rotating heliostats require larger land areas for movement and add mechanical complexity, which may increase cost and maintenance compared to conventional systems. A systematic comparison of the flux peaks is presented in Table 6.

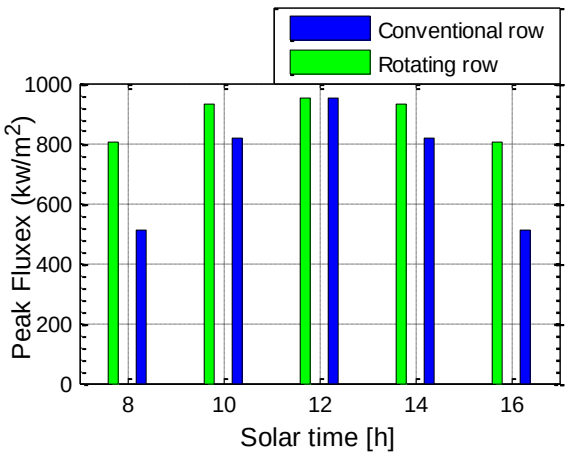

Figure 16. Variation of the superimposed peak flux values at the receiver's midpoint for different solar times (08:00, 10:00, 12:00, 14:00, and 16:00) during the spring equinox, comparing the first row of the PS10 solar power plant in Spain to an equivalent rotating solar field concept.

Table 6. Peak flux comparison of conventional and rotating heliostat rows

Specific times of spring equinox day		8h.00 and 16h.00	10h.00 and 14h.00	12h.00
Peak fluxes (kW/m^2)	Conventional row	512.74	815.24	950.81
	Rotating row	804.35	930.45	950.81
Difference %		36.25	12.38	0.00

4. Conclusion and perspectives

The work in this paper presents a comparison of the peak flux density distribution produced by two different technologies, namely conventional and rotating heliostats using a limited number of these devices to optimize the solar of the flux distribution on the receiver's image plane. The heliostats under investigation are well suited for the model developed based on the HFLCAL technical method, which was validated against experimental data. The geometric center coordinates of the heliostats of the PS10 solar power plant are reviewed to be adapted to the rotating field concept. Field simulation evaluates the amount of improved solar energy collection using rotating heliostat leading to more stable and higher cosine efficiency that overcomes the limitations of conventional heliostats. Furthermore, the map of the solar flux density distribution that gets the receiver image plane sent by the two types of technologies governing heliostats are compared in the same location at five separate moments on the spring equinox day. The comparison is done for a single heliostat and a group of nine (09) heliostats distributed on the first row of the field for each type of technology. The first row of the PS10 power plant was chosen as the fundamental setup for our study, and here is where the data came from. According to the results, the 36.25% increase at 8 a.m. in the peak flux density distribution, obtained by the heliostats that adapt to the rotating row concept, compared to the conventional row of heliostats, diminishes in proportion to the sun's sky trajectory. When it reaches its maximum altitude, the peak flux value is the same for both kinds of concepts. A similarity is observed in the evolution of the peak fluxes of the two concepts relative to noon throughout the day. The advantage of the rotating heliostat concept is particularly significant in the morning and afternoon when the sun is at lower angles, as they reduce the cosine effect and achieves higher and more uniform peak flux throughout the day on the receiver. This improvement enhances optical efficiency and demonstrates the potential for real-world application in solar power tower plants, including better energy capture and reduced shading, since the heliostats have mobile foundations and are not fixed like conventional heliostats. While these benefits are notable, considerations such as design simplicity and cost remain important for practical implementation. Future work will extend this study to multi-row heliostat fields, optimize field layouts for different locations, and assess economic feasibility for large-scale deployment.

Nomenclature

A_m	Total mirror area of heliostat(m^2)
$cosrec$	Cosine of the angle between the reflected ray and the normal to the receiver surface (°)
D	Distance between the heliostat centre and the receiver center (m)
d	Square root of the whole heliostat area (m)
F_r	Distribution of the flux density on the receiver (Kw/m^2)
f	Focal distance of heliostat (m)
H_t	Image dimensions in the tangential plane(m)
I_D	Direct normal irradiation (Kw/m^2)
LH	Height of the heliostat (m)
LW	Width of the heliostat (m)
P_t	Power reflected by heliostat (Kw)
W_s	Image dimensions in the sagittal plane (m)
X, Y, Z	Cartesian coordinates (m)
$\vec{n}$	Unit vector normal of the surface of the heliostat
$\vec{r}$	Unit vector pointing to the receiver surface
$\vec{s}$	Unit vector pointing to the sun
ω_i	Incidence angle (°)
σ_{ast}	Astigmatic error (mrad)
σ_{bq}	Beam quality error (mrad)
σ_{HF}	The effective deviation (mrad)
σ_s	Slope error (mrad)
σ_{sun}	Sun shape error (mrad)
σ_t	Tracking error (mrad)
η	Instantaneous optical efficiency of the heliostat field
η_{att}	Atmospheric attenuation factor
η_{cos}	Cosine efficiency
η_{itc}	Interception factor
η_{ref}	Heliostat reflectivity factor
η_{sb}	Shading and blocking efficiency

References

1. He, Y.-L., et al., *Review of the solar flux distribution in concentrated solar power: Non-uniform features, challenges, and solutions.* Applied Thermal Engineering, 2019. **149**: p. 448-474. https://doi.org/10.1016/j.applthermaleng.2018.12.006
2. Gallego, A. and E.F. Camacho, *On the optimization of flux distribution with flat receivers: A distributed approach.* Solar Energy, 2018. **160**: p. 117-129. https://doi.org/10.1016/j.solener.2017.12.008
3. Oliveira, M., et al., *Solar radiation measurement tools and their impact on in situ testing—A Portuguese case study.* 2024. https://doi.org/10.3390/buildings14072117
4. Reddy, V.S., et al., *State-of-the-art of solar thermal power plants—A review.* Renewable and Sustainable Energy Reviews, 2013. **27**: p. 258-273. https://doi.org/10.1016/j.rser.2013.06.037
5. Collado, F.J. and J. Guallar, *Campo: Generation of regular heliostat fields.* Renewable energy, 2012. **46**: p. 49-59. https://doi.org/10.1016/j.renene.2012.03.011
6. Hu, P. and W. Huang, *Performance analysis and optimization of an integrated azimuth tracking solar tower.* Energy, 2018. **157**: p. 247-257. https://doi.org/10.1016/j.energy.2018.04.044
7. Maiga, M., et al., *Sources of solar tracking errors and correction strategies for heliostats.* Renewable and Sustainable Energy Reviews, 2024. **203**: p. 114770. https://doi.org/10.1016/j.rser.2024.114770
8. Belgasim, B., et al., *The potential of concentrating solar power (CSP) for electricity generation in Libya.* Renewable and sustainable energy reviews, 2018. **90**: p. 1-15. https://doi.org/10.1016/j.rser.2018.03.045
9. Merchán, R., et al., *High temperature central tower plants for concentrated solar power: 2021 overview.* Renewable and Sustainable Energy Reviews, 2022. **155**: p. 111828. https://doi.org/10.1016/j.rser.2021.111828
10. Bouamra, M. and M. Merzouk, *Cosine efficiency distribution with reduced tower shadowing effect in rotating heliostat field.* Arabian Journal for Science and Engineering, 2019. **44**: p. 1415-1424. https://doi.org/10.1007/s13369-018-3558-7
11. Behar, O., A. Khellaf, and K. Mohammedi, *A review of studies on central receiver*

solar thermal power plants. Renewable and sustainable energy reviews, 2013. **23**: p. 12-39. https://doi.org/10.1016/j.rser.2013.02.017

12. Wang, K., et al., *A novel integrated simulation approach couples MCRT and Gebhart methods to simulate solar radiation transfer in a solar power tower system with a cavity receiver.* Renewable Energy, 2016. **89**: p. 93-107. https://doi.org/10.1016/j.renene.2015.11.069
13. Rizvi, A.A., et al., *A review and classification of layouts and optimization techniques used in design of heliostat fields in solar central receiver systems.* Solar energy, 2021. **218**: p. 296-311. https://doi.org/10.1016/j.solener.2021.02.011
14. Lee, K. and I. Lee, *Optimization of a heliostat field site in central receiver systems based on analysis of site slope effect.* Solar Energy, 2019. **193**: p. 175-183. https://doi.org/10.1016/j.solener.2019.09.027
15. Arrif, T., et al., *Optimisation of heliostat field layout for solar power tower systems using iterative artificial bee colony algorithm: a review and case study.* International Journal of Ambient Energy, 2021. **42**(1): p. 65-80. https://doi.org/10.1080/01430750.2018.1525581
16. Ruiz, V., et al., *The variable geometry central receiver system concept. First results and comparison with conventional central receiver systems.* Energy Procedia, 2014. **57**: p. 2255-2264. https://doi.org/10.1016/j.egypro.2014.10.233
17. Cádiz, P., et al., *Shadowing and blocking effect optimization for a variable geometry heliostat field.* Energy procedia, 2015. **69**: p. 60-69. https://doi.org/10.1016/j.egypro.2015.03.008
18. Bouamra, M. and M. Merzouk. *Cosine Efficiency Distribution of Rotating Heliostat Field*. in *2017 International Renewable and Sustainable Energy Conference (IRSEC)*. 2017. IEEE. https://doi.org/10.1109/IRSEC.2017.8477337
19. Schöttl, P., et al., *Efficient modeling of variable solar flux distribution on Solar Tower receivers by interpolation of few discrete representations.* Solar Energy, 2018. **160**: p. 43-55. https://doi.org/10.1016/j.solener.2017.11.028
20. Collado, F.J., *One-point fitting of the flux density produced by a heliostat.* Solar energy, 2010. **84**(4): p. 673-684. https://doi.org/10.1016/j.solener.2010.01.019
21. He, C., Y. Zhao, and J. Feng, *An improved flux density distribution model for a flat heliostat (iHFLCAL) compared with HFLCAL.* Energy, 2019. **189**: p. 116239. https://doi.org/10.1016/j.energy.2019.116239
22. Salomé, A., et al., *Control of the flux distribution on a solar tower receiver using an optimized aiming point strategy: Application to THEMIS solar tower.* Solar energy, 2013. **94**: p. 352-366. https://doi.org/10.1016/j.solener.2013.02.025
23. Besarati, S.M. and D.Y. Goswami, *A computationally efficient method for the design of the heliostat field for solar power tower plant.* Renewable energy, 2014. **69**: p. 226-232. https://doi.org/10.1016/j.renene.2014.03.043
24. Raj, M. and J. Bhattacharya, *Precise and fast spillage estimation for a central receiver tower based solar plant.* Solar Energy, 2023. **265**: p. 112103. https://doi.org/10.1016/j.solener.2023.112103
25. Lipps, F. and M. Walzel, *An analytic evaluation of the flux density due to sunlight reflected from a flat mirror having a polygonal boundary.* Solar Energy, 1978. **21**(2): p. 113-121. https://doi.org/10.1016/0038-092X(78)90038-5
26. Collado, F.J., A. Gómez, and J. Turégano, *An analytic function for the flux density due to sunlight reflected from a heliostat.* Solar Energy, 1986. **37**(3): p. 215-234. https://doi.org/10.1016/0038-092X(86)90078-2
27. He, C., et al., *Analytical radiative flux model via convolution integral and image plane mapping.* Energy, 2021. **222**: p.

119937. https://doi.org/10.1016/j.energy.2021.119937

28. Atif, M. and F.A. Al-Sulaiman, *Optimization of heliostat field layout in solar central receiver systems on annual basis using differential evolution algorithm.* Energy conversion and management, 2015. **95**: p. 1-9. https://doi.org/10.1016/j.enconman.2015.01.089
29. Besarati, S.M., D.Y. Goswami, and E.K. Stefanakos, *Optimal heliostat aiming strategy for uniform distribution of heat flux on the receiver of a solar power tower plant.* Energy Conversion and Management, 2014. **84**: p. 234-243. https://doi.org/10.1016/j.enconman.2014.04.030
30. Collado, F.J. and J. Guallar, *A review of optimized design layouts for solar power tower plants with campo code.* Renewable and Sustainable Energy Reviews, 2013. **20**: p. 142-154. https://doi.org/10.1016/j.rser.2012.11.076
31. Atif, M. and F.A. Al‐Sulaiman, *Development of a mathematical model for optimizing a heliostat field layout using differential evolution method.* International Journal of Energy Research, 2015. **39**(9): p. 1241-1255. https://doi.org/10.1002/er.3325
32. Biencinto, M., J. Fernández-Reche, and A.L. Ávila-Marín, *HEFESTO: A novel tool for fast calculation and preliminary design of heliostat fields.* Renewable Energy, 2025. **245**: p. 122736. https://doi.org/10.1016/j.renene.2025.122736
33. Zhang, M., et al., *An efficient code to optimize the heliostat field and comparisons between the biomimetic spiral and staggered layout.* Renewable energy, 2016. **87**: p. 720-730. https://doi.org/10.1016/j.renene.2015.11.015
34. Saghafifar, M., K. Mohammadi, and K. Powell, *Design and analysis of a dual-receiver direct steam generator solar power tower plant with a flexible heliostat field.* Sustainable Energy Technologies and Assessments, 2020. **39**: p. 100698. https://doi.org/10.1016/j.seta.2020.100698
35. Huang, W. and L. Yu, *Development of a new flux density function for a focusing heliostat.* Energy, 2018. **151**: p. 358-375. https://doi.org/10.1016/j.energy.2018.03.035
36. Sattler, J.C., et al., *Review of heliostat calibration and tracking control methods.* Solar Energy, 2020. **207**: p. 110-132. https://doi.org/10.1016/j.solener.2020.06.030